UNIVERSITY OF CALIFORNIA SAN DIEGO

Visualize H3K27me3 and Caspase3 Activities during Apoptosis by Using FRET biosensors

A Thesis submitted in partial satisfaction of the

requirements for the degree

Master of Science

in

Bioengineering

by

Chujun Wei

Committee in Charge:

Professor Yingxiao Wang, Chair
Professor Jesse Jokerst
Professor Lingyan Shi

2020

The Thesis of Chujun Wei is approved, and it is acceptable in quality and form for publication on microfilm and electronically:

Chair

University of California San Diego

2020

Table of Contents

List of Figures/Tables

Acknowledgements

I would like to acknowledge Dr. Yingxiao Wang for his invaluable guidance, support as my principal investigator and the chair of my committee. Also, I would like to acknowledge Dr. Shaoying Lu for her help in data analysis, Ya Gong for her excellent training and mentorship, Jiaming Wei for her help in writing thesis, and all other lab members that had given me precious advice for my graduate study.

At last, I want to thank all my friends and my parents. None of this would have been possible without their unyielding support and encouragement.

Abstract of the Thesis

Visualize H3K27me3 and Caspase3 Activities during Apoptosis by Using FRET biosensors

by

Chujun Wei

Master of Science in Bioengineering

University of California San Diego, 2020

Professor Yingxiao Wang, Chair

Histone modifications play significant roles in many cellular processes, including cell cycle regulation, stress responses, cell fate decisions, and cell development and differentiation.[44] H3 lysine 27 trimethylation is a repressive histone modification regulated by methyltransferase enzyme EZH2 and demethylases KDM6.

Previous research shows that staurosporine resulted in the cleavage of caspase-3, decrease of cell viability and decrease of histone H3 lysine 27 trimethylation (H3K27me3)[1]. However, this process has not been visualized in living cells and the mechanism of caspase-3 substrate proteins that lead to the H3K27me3 decline have not been fully specified yet. In this paper, we monitored the dynamics of H3K27me3 and caspase-3 in HeLa cells via engineered caspase-3 NES FRET biosensor and H3k27me3 FRET biosensor. Imaging results intuitively revealed the dynamic decrease of H3K27me3 as a consequence of caspase-3 activation, which is consistent with previous findings. Caspase-6 and lamin A were the downstream proteins of caspase-3 involved in this process and by inhibiting caspase-6, the un-cleaved lamin A accelerated the decline of H3K27me3 during apoptosis. We hypothesize that caspase-3 activation induces the downregulation of EZH2 and the upregulation of KDM6, which ultimately leads to the diminish of H3K27 tri-methylation. Furthermore, the lack of lamin A disrupts the heterochromatin-lamina interaction, leading to the reduced accessibility of H3K27me3 by KDM6 and therefore a decreased rate of demethylation.

1. Background

1.1 Histone modifications and histone methylation

DNA carries genetic information that defines the fundamental characteristics of organisms. While the length of stretched DNA in a human cell is around 2 meters, the diameter of a nucleus is only around 6 μm. [2] It is therefore extremely challenging to organize the entire DNA strands in the nuclear structure.[2]

In eukaryotes, DNA double helix is tightly bound to histone protein particles and then form nucleosomes, which are the basic unit of chromosome. In order to allow DNA to become compact and accessible to the enzymes for replication, recombination and repair, histone not only acts as a DNA scaffold that wraps it around but also plays an important role in gene regulation via post-transcriptional modification of histone. Modification of histone tails changes nucleosomes spacing or recruitment of histone modifiers and finally leads to alternative gene expression, which includes methylation, phosphorylation, acetylation, ubiquitylation and sumoylation of the five major families: H1/H5, H2A, H2B, H3, and H4.[3]

Histone methylation modifies certain amino acids by adding methyl groups, which occurs predominantly on histone H3 and H4 targeting either arginine(R) or lysine(K) residues. Regarding single lysine, not only the three methylation levels: mono-, di- or tri-methylation but also the variation of residue sites could lead to distinctive effects on chromatin function. For example, H3K4 trimethylation is involved in active gene transcription. However, H3K27 trimethylation is involved in transcriptional silencing while heterochromatin formation and histone methyltransferase(HMTs) Enhancer of zeste homolog (EZH2) are recruited. [4,5] With the help of histone coiling, DNA is compacted in a way that can easily become available, and gene transcription can be regulated under different circumstances.

1.1.1 Role of Histone H3 lysine 27 trimethylation and EZH2

Previous research observed that the H3K27me3 at the target promoter was catalyzed by EZH2 via addition of methyl group resulting in downregulating expression of tumor suppressor genes and upregulating oncogenes. [6,7] Therefore, the overexpression of EZH2 and high level of H3K27me3 lead to hyperactivation of cancer cells, including cell survival, proliferation and invasion. [6,7]

Polycomb group (PcG) proteins contain two multi-complexes: Polycomb Repressive Complexes 1(PRC1) and 2(PCR2), which contain a catalytic subunit EZH2, embryonic ectoderm development (EED) and suppressor of zeste 12 (SUZ12). EZH2 constructs in specific structural motifs and contains several key domains, which are needed to maintain its normal function as histone methyltransferase (HMTs). An SET domain at the C-terminus maintains HMT's activity, trimethylated H3K27, silence targeted genes and involvement in various biological functions. The ncRBD and CXC domain are function as linker to connect regulatory proteins and PRC2 components. [8,9] After recruitments of SUZ12, EED and EZH2 and the addition of tri-methyl group to H3K27, PRC1 catalyze lysine 110 mono-ubiquitylation (K119) of histone H2A, and H2AK119Ub 1 result in compaction of chromatin and inhibition of transcriptional elongation.[10,11]

1.2 Apoptosis and caspase-3 apoptosis pathways

Apoptosis is defined by distinct morphological changes including cell and nucleus volume shrinkage, cell fragmentation, chromatin condensation, blebbing and apoptotic bodies formation, and energy-dependent biochemical mechanisms that stimulated by a group of cysteine proteases

caspase and cause a cascade of molecular events before cell death. [12,13,14] There are two main apoptotic pathways: extrinsic and intrinsic, and both of them converge into the same execution pathway which is activated by the cleavage of Caspase-3.

The extrinsic pathway initiates apoptosis by using extracellular signals that stimulate transmembrane receptor-mediated interactions. This process involves with cell death signals including the Fas ligand, TNF-related apoptosis inducing ligands, and tumor necrosis factor(TNF), which bind to death receptors. [15] After the adaptor death domain is recruited, death-inducing signaling complex(DISC) is composed of initiator procaspases-8 and -10 which bind to the adaptor protein. Execution Caspase-3, -6 and -7 are activated once the caspase-8 is cleaved by DISC and start cleavage of proteins and the cytoskeleton resulting in cell death.[16,17]

In this paper, we focus on using Staurosporine(STS) as a death stimulus to trigger caspase-3 programmed cell death.

1.2.1 Roles of lamin A

Even though caspase-6 and -7 have similar significant sequences as caspase-3, they are downstream caspase effectors of caspase-3 and play relatively minor or highly specialized roles.[18] Fodrin, gelsolin and RB are substrates that are directly cut by globally primary executioner caspase-3, while, lamin A and PARP are the major substrates that are targeted by caspase-6 and -7.[18] As a consequence, we used a caspase-6 inhibitor to protect Lamin A from degradation.

Lamin A is one of the major component that makes up nuclear lamina, the filamentous structure that lies underneath the inner nuclear membrane regulating chromatin dynamics [19,20]. It is essential in both maintaining mechanical and genomic stability through DNA double-strand

break(DSB) repair process and embryonic differentiation [21,22]. A genetic point mutation of Lamin A could cause Hutchinson–Gilford progeria syndrome (HGPS), an uncommon genetic disorder resulting in accelerated aging in children. It activates the cryptic splicing site near the C-terminus of prelamin A mRNA and causes the deletion of a 150-base-long RNA fragment which includes a protein that promotes the formation of mature lamin A [23,24,25]. Thus, the shortage of normal mature lamin A in HGPS patients in consequence of accumulated DNA damages, chromosomal instability, faster cell replication, accelerated aging with a relatively short life expectancy of 14 years.[26-33].

1.3 Fluorescence Resonance Energy Transfer Biosensors

Fluorescence resonance energy transfer(FRET) is a physical process in which an excited molecular fluorophore, the donor, transfers nonradioactive energy to another fluorophore, the acceptor.[34] This intermolecular dipole-dipole coupling depends on proper spectral overlap, the distance between the fluorophores, and the relative orientation of the fluorophore's transition dipole moments which makes FRET a spatiotemporal sensitive technique for detecting the changes in molecular proximity during biological events.[34] By utilizing FRET in genetically encoded biosensors, we can study the activity of cellular signaling molecules, protein interactions, and characterization of gene expression in living cell imaging via using this technique. [35,36]

1.3.1 17mer-linker H3K27me3 biosensor

In order to better visualize the tri-methylation modification at lysine position 27 on histone H3 in living cell, our lab successfully constructed a FRET biosensor based on Alice Ting group's design with accurate localization and enhanced FRET contrast compared to its basal level. By

adjusting the linker length and the binding affinity, we finalized our design with truncated Drosophila Polycomb (Pc) chromodomain, a full-length histone H3 containing the lysine K27 position and fluorophores ECFP and YPet linked by 17mer-linker.[44] (Figure 1A)

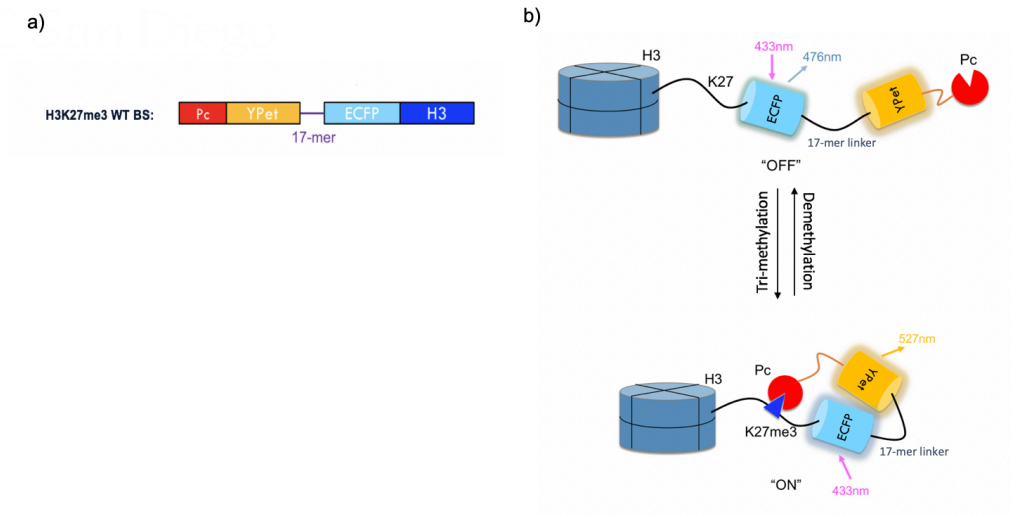

Figure 1: Construction of H3K27me3 FRET biosensor. A) Map of H3K27me3 WT biosensor. B) Schematic presentation of the FRET mechanism of the H3K27me3 WT biosensor in cells. Adapted from Gong Ya's thesis. [44]

At the resting stage, fluorescent pairs are too far to cause FRET energy transfer. While H3K27 trimethylation occurs, the PC chromodomain binds to the H3K27me3 substrate to shorten the distance between the fluorescent protein pairs and cause FRET change(Figure 1B). This is a reversible activity, therefore, the change of FRET ratio, $\frac{ECFP}{YPet\ FRET}$ reflects on the alternation of global tri-methylation level on H3K27me3.[44] In order to have a negative control, a mutation on Y26 from the aromatic ring side chains to lysine was introduced in Pc chromodomain resulting in sensor and ligand recognition and binding failure. From experimental data shown in Gong's paper, we confirmed that the FRET ratio in the H3K27me3 WT biosensor was significantly higher than the H3K27me3 Y26K biosensor.[44] Therefore, in this research, we used WT biosensor to detect H3K27me3 global activity and used Y26K as a negative control during caspase-3 programmed cell death.

1.3.2 Caspase-3 FRET biosensor

Caspase-3 FRET biosensor constructs containing fluorescent protein pairs LSSmOrange (excitation/emission at 437/572nm) linked by a 20 amino acid processing caspase-3 recognition site, DEVD, to mKate2(excitation/emission at 460/605nm).(Figure 2A) [37] At the resting stage, LssmOrange and mKate2 are close enough to have FRET signal. While, by adding staurosporine, the activation of caspase-3 is accompanied by a parallel increase in cleavage of the introduced caspase-3 FRET biosensor at DEVD site, resulting in the change of spatial arrangement of the LSSmOrange and mKate 2. (Figure 2B)[38]

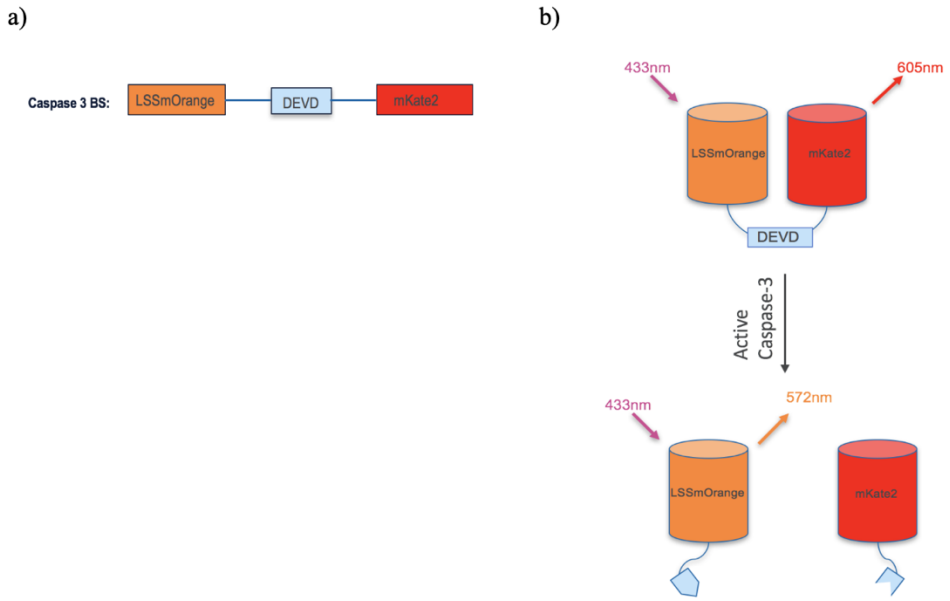

Figure 2: Construction of Caspase-3 FRET biosensor. a) Map of Caspase-3 FRET biosensor.
b) Schematic presentation of the FRET mechanism of the Caspase-3 FRET biosensor in cell. Adapted from [38].

1.3.3 Dual FRET pairs

LssmOrange fills up an existing spectral gap and applies to simultaneously image two FRET pairs by using single excitation wavelength. However, caspase-3 FRET Biosensor localizes in the whole cell and causes some minor overlapping signal while coupling with

H3K27me3 FRET biosensor because some microscopy channels capture both of the signals emitted from fluorophores LSSmOrange and YPet. Therefore, we engineered and constructed a caspase-3 FRET biosensor with nuclear export signal (NES) at C-terminal to compare them. In consequence, we can monitor the H3K27me3 and apoptotic activity at the same time in a single cell by using LSSmOrange-mKate2 and ECFP-YFP and measuring the FRET ratio change of these two biosensors.

2. Results

2.1Construction and imaging verification of caspase-3 NES FRET biosensor

In order to visualize the dynamics of caspase-3 and H3K27me3, corresponding biosensors were used in live cell imaging. For the H3K27me3 WT biosensor, the fluorescent pairs were ECFP (excitation 434nm, emission 477nm) and YPet (excitation 517nm, emission 530nm). For caspase-3 biosensor, the fluorescent pairs were LSSmOrange (excitation 437nm, emission 572nm) and mKate2 (excitation 588nm, emission 633nm). Because the emission wavelength of Ypet and LSSmOrange fell into the same range of some filters, the mixture of signals from two biosensors were captured. For example, in LSSmOrange channel (575nm DF20), it majorly received emission signal from LSSmorange but part of YPet signal was captured which should not happen ideally. Even though one of the biosensors is dominant, FRET biosensor is a sensitive tool and a small effect could lead to inaccuracy. Therefore, we decided to separate the two biosensors spatially to minimize this type of error.

H3K27me3 biosensor contained a nuclear localization signal (NLS) in the H3 domain and could efficiently localize into the nucleus. Hence, we reconstructed the caspase-3 biosensor by inserting a nuclear localization signal (NES) sequence which prevented it from getting into

the nucleus. When the caspase-3 was inactive, LSSmOrange and mKate2 were linked by DEVD so the FRET signal was generated. When caspase-3 was active and able to cleave DEVD, the fluorophores separated and then the FRET signal was lost (Figure 3A).

After successfully constructing the biosensor, we transiently transfected caspase-3 biosensor or caspase-3 NES biosensor into HeLa cells. We took a 500 minutes time series imaging and added 2uM staurosporine at 20 minutes for both groups of cells. Compared with caspase-3 biosensor, the construct with NES were efficiently located in cytoplasm and did not cause any significant effect on the viability and conditions of the cells. Only the signals within the selected area (red circle) were captured, meanwhile the $\frac{\text{LSSmOrange}-\text{mKate2 FRET}}{\text{LSSmOrange}}$ ratio was generated from the quantitative measurement of emission wavelengths acquired by these two channels (Figure 3c). From the normalized FRET ratio, both biosensors presented similar trends and decreased within 200 to 350 minutes (Figure 3c). Even though the FRET ratio of caspase-3 biosensor had a larger decrease in quantity, the drop of caspase-3 NES biosensor was sufficient to indicate the activation of caspase-3 and the FRET Ratio change in terms of time was major concern in the following experiments.

After solving the signal overlapping problem, we combined caspase-3 NES biosensor and H3K27me3 biosensor to visualize the dynamic change of H3K27me3 during caspase-3 programmed cell death.

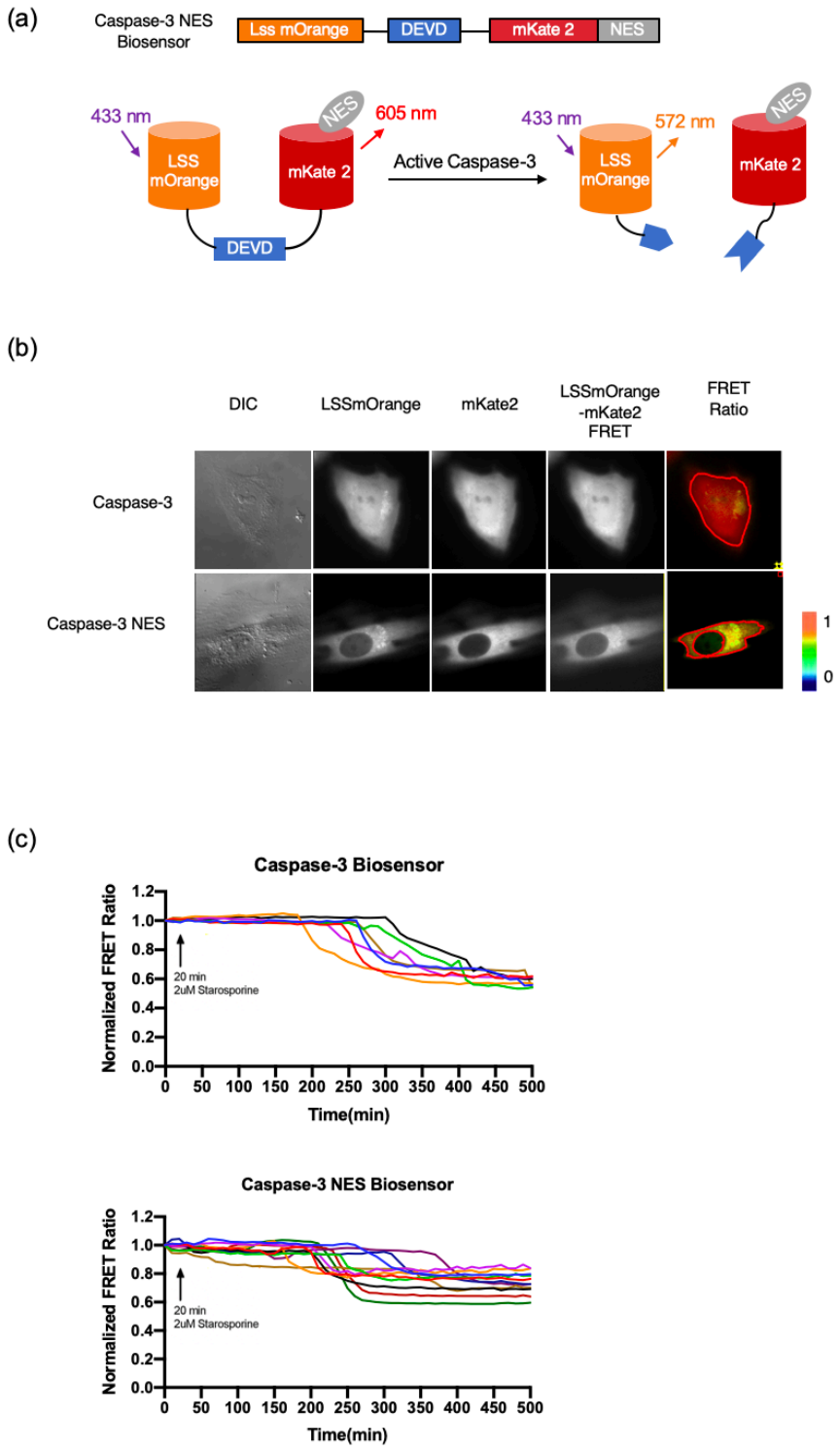

Figure3: Construction and imaging verification of caspase-3 NES FRET biosensor. a) Map and schematic of caspase-3 NES FRET Biosensor with NES sequences inserted at -C terminal. b) HeLa cells transiently transfected with caspase-3 biosensor or caspase-3 NES biosensor and took a 500 minutes imaging with 20μM of staurosporine added at 20 minutes. Representative images of cells at t=0 minutes in DIC, LSSmOrange, mKate2, LssmOrange-mKate2 FRET channels and LssmOrange-mKate2 FRET Ratio. c) Normalized FRET Ratio trend of caspase-3 biosensor with or without NES.

2.2 Imaging of caspase-3 NES biosensor with H3K27me3 WT or Y26k biosensor

HeLa cells were transiently co-transfected with H3K27me3 WT biosensor and caspase-3 NES biosensor in 2:1ratio. After 48 hours, cells were seeded on a glass bottom dish and monitored under microscope, with 10-minute time intervals for 400 minutes. At the beginning, the nuclear membrane was structurally normal and functionally complete, which separated the caspase-3 NES biosensor from the H3K27me3 WT biosensor. At 20 minutes, 20μM of STS was added into the cell, which activated caspase-3 and caused the cleavage of DEVD in caspase-3 NES biosensor (Figure 4a).

Within the first 160 minutes, both FRET ratios remained almost unchanged. After then, the cell slightly rounded up and detached from the surface, and the nuclear envelope started to fragment. Also, the FRET ratio of caspase-3 NES biosensor in the transfected HeLa cells gradually decreased with the decreasing LSSmOrange-mKate2 FRET fluorescence intensity and increasing LSSmOrange, compared with those before treatment. The FRET ratio reached the minimum at 240 minutes when the cell outlines become convoluted and form extensions. A more than 20% reduce of $\frac{\text{LSSmOrange}-\text{mKate2 FRET}}{\text{LSSmOrange}}$ ratio indicated that the occurrence of fusion protein LSSmOrange-DEVD-mKate2 cleavage, while H3K27me3 stayed almost the same. At around 320 minutes, the extensions spread, and the cell membrane warped with cellular organelles and nucleus fragments to form small blebs and apoptotic bodies. Starting from 290 minutes, the H3K27me3 level decreased moderately and reached the minimum FRET ratio at around 340 minutes, which suggested that the unbinding of K27me3 to Pc chromodomain with the decreasing of YPet FRET signal. At 400 min, the cell was disintegrating and the apoptotic bodies were rapidly phagocytosed into neighboring cells. As we can see, the time of H3K27me3 and caspase-3 started to drop is different but they followed the same trend. The time distance between them, Δt , is,

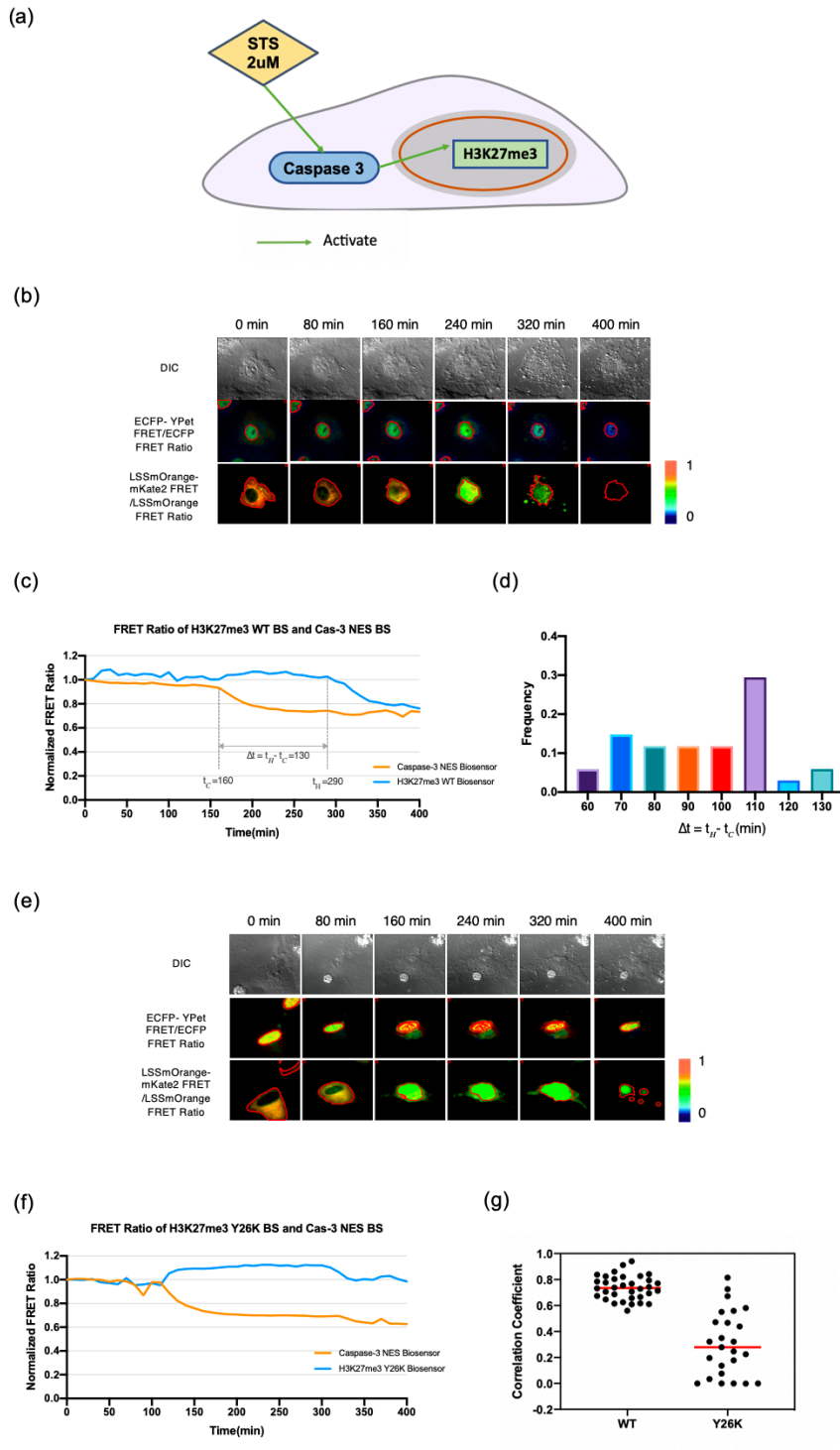

Figure 4, Imaging data and analysis of HeLa cells with caspase-3 NES biosensor and H3K27me3 WT or Y26k biosensor. Cells co-transfected with H3K27me3 WT or Y26K biosensor and Caspase-3 NES biosensor were visualized using a Nikon microscope in a 400 minutes time series and 10 minutes interval. 20μM of STS was added into cells at 20min after imaging. a) Overview of experimental plan. b) Representative images of HeLa cell in ECFP-YPET FRET Ratio showed the activity of H3K27me3 WT biosensor and LSSmOrange-mKate2 FRET Ratio showed activity of Caspase-3 NES biosensor. c) Graph shows the FRET ratios trend of two biosensors. Blue line represents H3K27me3 WT biosensor; Orange line represents Caspase-3 NES biosensor. Δt measures the time

distance between t_H, the point that ECFP/ YPet FRET ratio started to drop and the point t_c that LSSmOrange-mKate2 FRET/ LSSmOrange started to drop. d)Histogram of t for a total 34 HeLa cells. e) Representative images of HeLa cell double transfected with H3K27me3 Y26K biosensor and Caspase-3 NES biosensor. E) Graph of the FRET ratio trends for H3K27me3 level observed from H3K27me3 Y26K biosensor and Caspase-3 activity.

$\Delta t = t_H - t_c = 290 - 160 = 130$ minutes for this cell. It revealed that the time for H3K27me3 to react to the apoptosis is 130 min after caspase-3 activation. Due to the FRET ratio trends for both biosensors were similar, we used cross-correlation function in Matlab to analyze the time displacement of H3K27me3 FRET ratio relative to caspase-3's with correlation coefficient above 0.6. Histogram in figure 2d showed the time distance of 34 cells in the range of 60 minutes to 140 minutes with mean 97.3 minutes, mode 110 minutes and median 100 minutes.

In order to confirm the dynamic observed from H3K27me3 WT biosensor reflected to the real biological change of H3K27me3 in chromatin, a negative control experiment was done with same setting except we used mutated version of H3K27me3 instead of WT. A mutation on Y26 to lysine was introduced to the Pc domain, which was expected to cause the unrecognition between Pc domain and K27me3, therefore, there should be no change in FRET ratio during caspase-3 apoptosis. H3K27me3 Y26K biosensor and caspase-3 NES biosensor were co-transfected into HeLa cells in ratio 2:1 and imaged after 48 hours. Activity of Caspase-3 and cell in DIC channel exhibited same behavior as experimental group that caspase-3 gradually drop around 110 minutes and cell went through the morphological changed under apoptosis, for example cell shrinkage, nuclear membrane fragmentation, membrane blebbing and so on. The difference from the experimental group is that the H3K27me3 FRET ratio observed from the H3K27me3 Y26K biosensor stayed almost unchanged compared to the cell before STS treatment. By using cross-correlation to analysis data, we found out the average correlation coefficient was 0.3 which indicated that the signal observed from H3K27me3 Y26K biosensor did not have significant correlation to the caspase-3 activity.

By comparing the results from the experimental group with the control group, we confirmed that H3K27me3 decrease followed by the activated caspase-3 in STS induced caspase-3 apoptosis.

2.3 Imaging of caspase-3 NES biosensor with H3K27me3 WT biosensor with caspase-6 inhibitor

As shown in the relationship chart , caspase-6 is the downstream caspase effectors of caspase-3 and its activation would directly lead to the cleavage of Lamin A (Figure 5a). Additionally, McCord RP's research suggested in Hutchinson-Gilford progeria syndrome (HGPS) fibroblasts, which lack mature Lamin A, the H3K27me3 level is lower than the health cell.

Based on previous research and conclusion draw from the first experiment, we further hypothesized that caspase-6 and Lamin A were the key component that connected caspase-3 and H3K27me3. Therefore, we used Z-VEID-FMK as a caspase-6 inhibitor to prevent the degradation of Lamin A while using STS to induce the activation of caspase-3.

We transiently transfect LaminA-mCherry construct into HeLa cells and treated with 100 μM of caspase-6 inhibitor for 3 hours in 37°C before imaging for the experimental group. Images were captured in the mCherry channel using Nikon 2 microscope for a 400 minutes and 10 minutes interval. At 20min after imaging began, 20μM of STS was added to experimental and control groups. The morphological change in the DIC channel revealed that these two groups of cells underwent caspase-3 apoptosis. At the beginning, the mCherry signal appeared insensitive on the edge of the nuclear membrane, indicating the location of Lamin A.

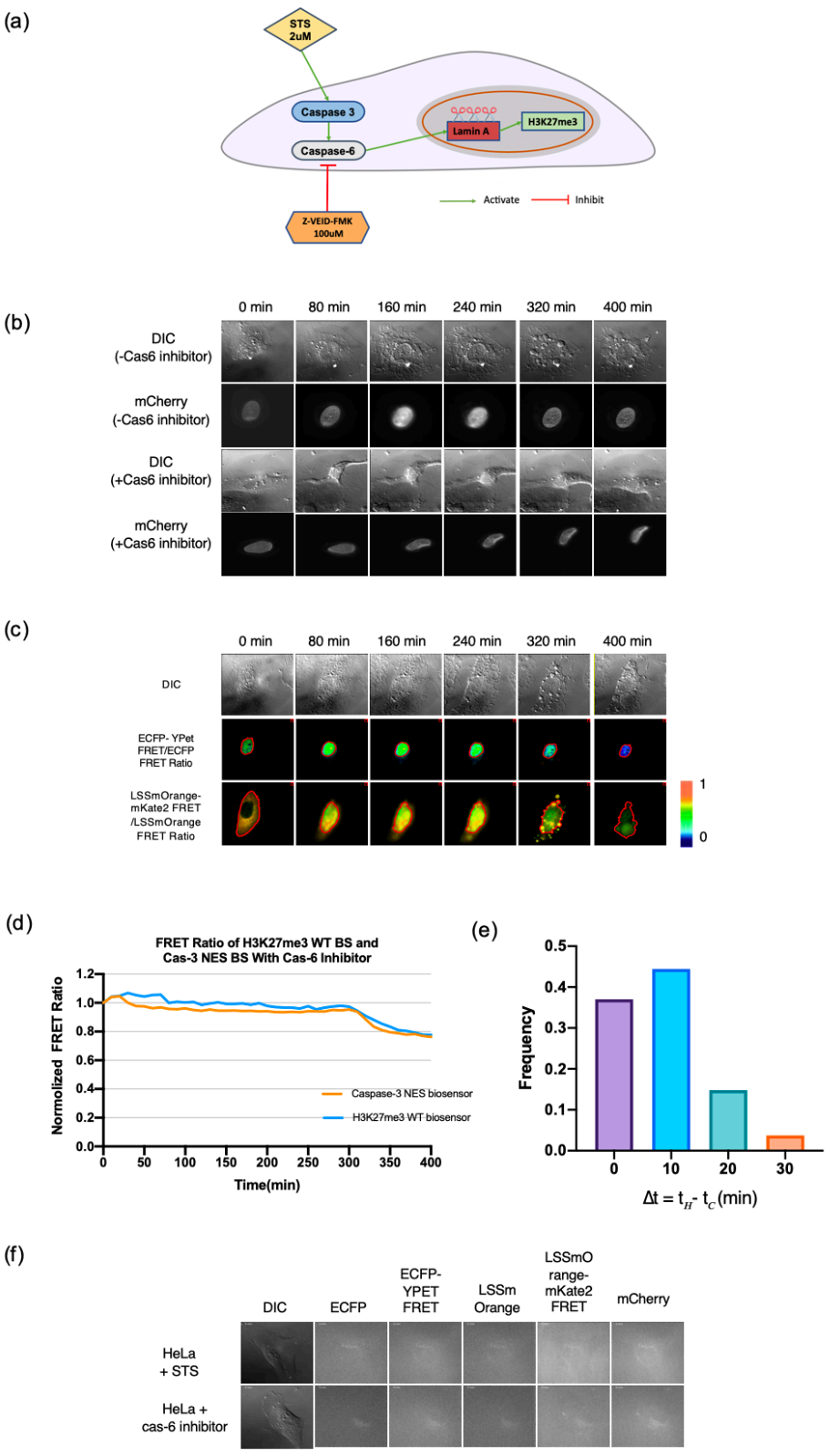

Figure 5. Imaging data and analysis of HeLa cells with H3K27me3 WT and caspase-3 NES biosensor treated with caspase-6 inhibitor. a) Relationship chart of the key component involved in H3K27me3 dynamic during caspase-3

apoptosis and experimental plan b) Representative cells images are shown in DIC and mCherry channels. LaminA-mCherry plasmids transiently transfect into cells. After 48 hours, treated them with or without caspase-6 inhibitor for 3 hours. c) Representative images of cells. HeLa cells double transfected with H3K27me3 WT biosensor and Caspase-3 NES biosensor were taken live cell imaging under Nikon 2 microscope for each 10-minute time interval for 400 minutes. Cells were treated with 100 μM of caspase-6 inhibitor for 3 hours in 37°C humidified-incubator with 5% CO_2 before imaging and 20μM of STS was added at 20min after imaging. d) FRET ratio change of H3K27me3 observed from H3K27me3 WT biosensor and caspase-3 observed from caspase-3 NES biosensor with caspase-6 inhibitor treatment for a representative cell. e) Histogram of Δt for total 27 HeLa cells calculated by using cross correlation function in Matlab. f) Negative control. Images of HeLa Cells treated with 100 μM of caspase-6 inhibitor for 3 hours in 37°C humidified-incubator with 5% CO2 before imaging and HeLa cells added 20μM of STS in different channels.

After STS was taking effect, caspase-3 was activated to cleave caspase-6, and in consequence Lamin A was cut without the caspase-6 inhibitor. Due to the split of Lamin A-mCherry, mCherry was no longer fixed to the nuclear membrane so we can see it floated freely in the nuclear from the brightness in the mCherry channel. Lamin A-mCherry is a constitutive biosensor which means the amounts of mCherry were constant in a cell. Therefore, the sudden brightness was due to the shrinkage of cell, concentrated mCherry and mCherry relocation by comparison with the Caspase-6 inhibitor treated cell. The unchanged of mCherry in the treatment group indicated that the caspase-6 inhibitor targeted the membrane associated protein Lamin A and successfully prevented it from cleavage (figure 5b).

Then we treated the HeLa cell with H3K27me3 WT biosensor and caspase-3 NES biosensor with 100 μM of caspase-6 inhibitor 3 hours before live cell imaging and 20μM of STS at 20 minutes after imaging. From DIC channels, we observed that HeLa cells experienced caspase-3 programmed cell death, starting from normal and flat shape to unattached and blebbing cells with apoptotic bodies. From figure 5e, the FRET ratio observed from H3K27me3 WT and caspase-3 NES biosensors changed simultaneously, which consists of cell images and both of them decreased gradually from 310 minutes with more than a 20% drop. For the representative cell, the time lag between H3K27me3 and caspase-3 activation is 0. By comparing the

correlation of FRET ratios for 27 cell samples using Matlab, Δt was shown in histogram with mean at 8.5 minutes, median at 10 minutes, and mode at 10 minutes.

3. Discussion

Hyun's research suggests that lysine methylation levels are precisely balanced by the action of methyltransferase as writers to add methyl groups and demethylases as erasers to take out methyl groups.[39] The loss of methyltransferase EZH2 and the gain of demethylases KDM6 lead to the net loss of global H3K27me3 level. Consistent with our result, He's research shows that caspase-3 activation leads to H3K27me3 level decrease due to the significant upregulation of KDM6A and KDM6B and downregulation of EZH2. [40] Other than the direct decrease of EZH2, some recruiter proteins required in the process of H3K27me3, such as retinoblastoma protein (pRB), were degraded during caspase-3 apoptosis, which further block the addition of methyl group. [41] In the early research, microscopy images exhibit the H3K27me3 location adjacent to the Lamin A's. [42] Later on, H3K27me3 was found out that it has a tight association with the nuclear lamina through lamina-associated domains. [43] Therefore, we hypothesize that, with the protection of caspase-6, Lamin A are complete and H3K27me3 is able to interact with nuclear lamina, making it easier for demethylases to locate and bind to H3K27me3, and remove the methyl group afterward. This series of processes ultimately results in the H3K27me3 level reduces faster in the group treated with caspase-6 inhibitor.

During the experiments, we observed that in some of the cells, as the caspase-3 FRET ratio declined, the H3K27me3 FRET ratio slightly increased but eventually went back and did not affect the overall trend. For example, in figure 2E, at 160 minutes, the caspase-3 FRET ratio dropped while the H3K27me3 FRET ratio increased. This is an unspecified event that happens randomly in different groups of HeLa cells. One possible reason might be the two biosensors

were no longer compartmentalized due to the nuclear membrane damaged during apoptosis. Therefore, in YPet channel, not only the YPet intensity was captured but also a part of the LSSmOrange result in the overall signal acquired from YPet channel was increased. Another reason might be the unspecific chromatin regulation was triggered when cell volume shrinks, nuclear condensed, morphology changes or dies….

In the future study, on the one hand, it would be interesting to further study the Δt in normal cells and HGPS cells which have Lamina A deficiency, in order to better understand the mechanism and the role Lamin A plays in the H3K27me3 during caspase-3 apoptosis. On the other hand, after validating that H3K27me3 FRET biosensor is a sensitive tool to monitor heterochromatin global H3K27me3 dynamic, we can further use it to monitor the local epigenetic changes at a specific genomic locus. We can trigger DSB (double strand DNA breakage) at a region of interest by chemical inducible CRISPR-associated protein 9 and indicate the region by engineered DSB binding protein with fluorophore, for example GFP-Ku. FRET biosensor was transfected into cells and detect the change around the DSB.

In conclusion, we found that caspase-3 activation led to the global H3K27me3 level decreasing. Caspase-6 and lamin A were the downstream proteins of caspase-3 involved in this process and the existence of inactivated caspase-6 and un-cleaved lamin A could have accelerated the decline of H3K27me3 during apoptosis. We predict that caspase-3 activation induced downregulation of EZH2 and upregulation of KDM6 which ultimately lead to diminishment of H3K27me3 and the lack of lamin A disrupted heterochromatin-lamina interaction which brings a difficulty for KDM6 to target H3K27me3.

4. Materials & Methods

4.1 Caspase-3 Biosensor Construct with Nuclear export signal(NES)

Inserting -NES DNA sequence(-ttagccttgaaattagcaggtcttgatatcgggagc-) into Caspase-3 Biosensor via polymerase chain reaction (PCR). Caspase-3 Biosensor plasmid (cat#60883) served as template reacts with two primers which included NES sequence and Q5 high-fidelity DNA polymerase (New England BioLabs, cat#: M0491L) during PCR. Purifying and extracting sample via DNA electrophoresis and gel extraction. DH5acompetent E. coli cells were used for transformation, heated shock for 35 second, recovered in SOC incubated at 37C for 1 hour and plated in agar plate with kanamycin antibiotic for overnight at 37C. Single colony grew in LB media with Kanamycin (1:5000 dilution) at 37C shaker for 12-16 hours. After amplification, mini-prep the sample via Quagent Kit resulted in concentrated Caspase3-NES biosensor plasmid. The model of the thermal cycler used was the Bio-Rad C1000 Touch^{TM} Thermal Cycler for PCR reactions.

4.2Cell Culture and Transient Transfection

HEK293 cells [American Tissue Culture Collection (ATCC) (Manassas, VA)] and HeLa cells were cultured in Dulbecco's modified Eagle medium (DMEM) (Gibco) supplemented with 10% fetal bovine serum (FBS) (Atlanta Biologicals, Lawrenceville, GA), and 1% penicillin/streptomycin (Invitrogen) in 37°C humidified-incubator with 5% CO_2. They were transiently transfected with the Caspase3 biosensor, Caspase3-NES biosensor, H3K27me3 WT biosensor, H3K27me3 Y26K biosensor or LaminA-mCherry plasmid using Lipofectamine 3000 kit (Sigma-Aldrich) 48 hours before imaging. HeLa cells at 70-90% confluent was double-

transiently transfected with Caspase3-NES biosensor and H3K27me3 WT or Y26K biosensor in 1:2 ratio.

4.3 Imagine Acquisition and Analysis

Cells were plated onto glass-bottom dishes (Cell E&G) coated with fibronectin (Sigma) at 10 μg/mL and diluted with PBS one night before imaging. Caspase-6 inhibitor (R&D Systems™ Caspase-6 Inhibitor Z-VEID-FMK) at final concentration of 100 μM was treated with cells 3 hours before imaging. Staurosporine(STS) was added to the cell at 20min, the gap between the second and third time frame at final concentration 20μM.

Nikon eclipse Ti inverted microscope with 100x DIC Nikon microscope objective (Numerical aperture1.4), a 300W Xenon lamp (Atlas Specialty Lighting), an electron-multiplying (EM) charge-coupled device camera (QuantEM:512SC, Photometrics) and MetaFluor Fluorescence Ratio Imaging Software (Molecular Devices) was used to collect microscopic images. Images were captured with a 420DF20 excitation filter, a 450DRLP dichroic mirror, and four emission filters controlled by a filter changer corresponding with six channels (475DF40 forECFP, 535DF25 forECFP-YPET FRET, 575DF20 for LssOrange, 630DF20 for LssOrangemKate2FRET, 630DF20 for mKate2). Dual FRET with single-wavelength excitation, LssOrangemKate2FRET setup with exposure 400ms andECFP-YPET FRET setup with exposure 600ms. Life imaging duration was 400 min, total 41 time points and every 10 min.

Imaging data were processed on FluoCell JAVA developed by the Wang lab. The background and noise signal were subtracted automatically. FRET ratio is an average value for a whole cell and was normalized by the value at the first frame (t=0). Cross-correlation function

was used to compare the trend and the similarity of two biosensors signals within one cell. All the code was generated via Matlab.

5. Reference

1. He, C., Sun, J., Liu, C., Jiang, Y., & Hao, Y. (2019). Elevated H3K27me3 levels sensitize osteosarcoma to cisplatin. Clinical Epigenetics, 11(1). doi:10.1186/s13148-018-0605-x

2. Alberts, B., Johnson, A., Lewis, J., Morgan, D., Raff, M. C., Roberts, K., Walter, P., Wilson, JH., Hunt, T. (2015). Molecular biology of the cell. New York, NY, NY: Garland Science.

3. Marullo, F., Cesarini, E., Antonelli, L., Gregoretti, F., Oliva, G., & Lanzuolo, C. (2016). Nucleoplasmic Lamin A/C and Polycomb group of proteins: An evolutionarily conserved interplay. Nucleus, 7(2), 103-111. doi:10.1080/19491034.2016.1157675

4. Guenatri M., Bailly D., Maison C., Almouzni G. (2004). Mouse centric and pericentric satellite repeats form distinct functional heterochromatin. J Cell Biol, 166(4), 493-505. doi:10.1083/jcb.200403109

5. Peterson, C. L., & Laniel, M. (2004). Histones and histone modifications. Current Biology, 14(14). doi:10.1016/j.cub.2004.07.007

6. Gan, L., Yang, Y., Li, Q., Feng, Y., Liu, T., & Guo, W. (2018). Epigenetic regulation of cancer progression by EZH2: From biological insights to therapeutic potential. Biomarker Research, 6(1). doi:10.1186/s40364-018-0122-2

7. Aier, I., & Raj, U. (2016). Exploring the role of EZH2 (PRC2) as epigenetic target. 2016 International Conference on Bioinformatics and Systems Biology (BSB). doi:10.1109/bsb.2016.7552131

8. Margueron, R., & Reinberg, D. (2011). The Polycomb complex PRC2 and its mark in life. Nature, 469(7330), 343-349. doi:10.1038/nature09784

9. Pasini D, Di Croce L.(2016). Emerging roles for Polycomb proteins in cancer. Curr Opin Genet Dev. 36:50-58. doi:10.1016/j.gde.2016.03.013

10. Francis, N. J. (2004). Chromatin Compaction by a Polycomb Group Protein Complex. Science, 306(5701), 1574-1577. doi:10.1126/science.1100576

11. Morey, L., & Helin, K. (2010). Polycomb group protein-mediated repression of transcription. Trends in Biochemical Sciences, 35(6), 323-332. doi:10.1016/j.tibs.2010.02.009

12. Norbury, C., & Hickson, I. (2001). Cellular responses to DNA damage. Annu Rev Pharmacol Toxicol, 41(367), 401st ser.

13. Arends, M. J., Morris, R. G., & Wyllie, A. H. (1990). Apoptosis. The role of the endonuclease. The American journal of pathology, 136(3), 593–608.

14. Curtin, J. F., & Cotter, T. G. (2003). Live and let die: Regulatory mechanisms in Fas-mediated apoptosis. Cellular Signalling, 15(11), 983-992. doi:10.1016/s0898-6568(03)00093-7

15. Locksley, R. M., Killeen, N., & Lenardo, M. J. (2001). The TNF and TNF Receptor Superfamilies. Cell, 104(4), 487-501. doi:10.1016/s0092-8674(01)00237-9

16. Elmore, Susan. (2007).Apoptosis: A Review of Programmed Cell Death. Toxicol Pathol. 35(4): 495–516

17. Pfeffer, C., & Singh, A. (2018). Apoptosis: A Target for Anticancer Therapy. International Journal of Molecular Sciences, 19(2), 448. doi:10.3390/ijms19020448

18. Elizabeth A. Slee, Colin Adrain and Seamus J. Martin.(2001). Executioner Caspase-3, -6, and -7 Perform Distinct, Non-redundant Roles during the Demolition Phase of Apoptosis. The Journal of Biological Chemistry.276, 7320-7326.

19. Aebi, U.; Cohn, J.; Buhle, L.; Gerace, L. (1986). The nuclear lamina is a meshwork of intermediate-type filaments. Nature. 323, 560− 564.

20. Bronshtein, I., Kepten, E., Kanter, I., Berezin, S., Lindner, M., Redwood, A. B., Mai, S., Gonzalo, S., Foisner, R. & Shav-Tal, Y. (2015). Loss of lamin A function increases chromatin dynamics in the nuclear interior. Nature Communications. 6 (1), 1-9.

21. Manju, K., Muralikrishna, B. & Parnaik, V. K. (2006). Expression of disease-causing lamin A mutants impairs the formation of DNA repair foci. Journal of Cell Science. 119 (13), 2704-2714.

22. Smith, E. R., Meng, Y., Moore, R., Tse, J. D., Xu, A. G., & Xu, X. (2017). Nuclear envelope structural proteins facilitate nuclear shape changes accompanying embryonic differentiation and fidelity of gene expression. BMC Cell Biology,18(1). doi:10.1186/s12860-017-0125-0

23. De Sandre-Giovannoli, A., Bernard, R., Cau, P., Navarro, C., Amiel, J., Boccaccio, I., Lyonnet, S., Stewart, C. L., Munnich, A. & Le Merrer, M. (2003). Lamin a truncation in Hutchinson-Gilford progeria. Science. 300 (5628), 2055.

24. Corrigan, D. P., Kuszczak, D., Rusinol, A. E., Thewke, D. P., Hrycyna, C. A., Michaelis, S. & Sinensky, M. S. (2005). Prelamin A endoproteolytic processing in vitro by recombinant Zmpste24. Biochemical Journal. 387 (1), 129-138.

25. Li, Bingbing X., Chen, Jingjin,. Chao, Bo,. Zheng, Yixian,. And Xiao, Xiangshu. (2018). A Lamin-Binding Ligand Inhibits Homologous Recombination Repair of DNA Double-Strand Breaks.ACS Central Science, 4 (9), 1201-1210 DOI: 10.1021/acscentsci.8b0037

26. Wang, Y., Lichter-Konecki, U., Anyane-Yeboa, K., Shaw, J. E., Lu, J. T., Östlund, C., Shin, J., Clark, L. N., Gundersen, G. G. & Nagy, P. L. (2016). A mutation abolishing the ZMPSTE24 cleavage site in prelamin A causes a progeroid disorder. J Cell Sci, 129 (10), 1975-1980.

27. Liu, Y., Rusinol, A., Sinensky, M., Wang, Y. & Zou, Y. (2006). DNA damage responses in progeroid syndromes arise from defective maturation of prelamin A. Journal of Cell Science, 119 (22), 4644-4649.

28. Musich, P. R. & Zou, Y. (2009). Genomic instability and DNA damage responses in progeria arising from defective maturation of prelamin A. Aging (Albany NY), 1 (1), 28.

29. Musich, P. R., & Zou, Y. (2011). DNA-damage accumulation and replicative arrest in Hutchinson–Gilford progeria syndrome. Biochemical Society Transactions, 39(6), 1764-1769. doi:10.1042/bst20110687

30. Liu, B., Wang, J., Chan, K. M., Tjia, W. M., Deng, W., Guan, X., Huang, J., Li, K. M., Chau, P. Y. & Chen, D. J. (2005). Genomic instability in laminopathy-based premature aging. Nature Medicine, 11 (7), 780-785.

31. Corrigan, D. P., Kuszczak, D., Rusinol, A. E., Thewke, D. P., Hrycyna, C. A., Michaelis, S. & Sinensky, M. S. (2005). Prelamin A endoproteolytic processing in vitro by recombinant Zmpste24. Biochemical Journal, 387 (1), 129-138.

32. Hennekam, R. C. (2006). Hutchinson–Gilford progeria syndrome: review of the phenotype. American Journal of Medical Genetics Part A, 140 (23), 2603-2624.

33. Manju, K., Muralikrishna, B. & Parnaik, V. K. (2006). Expression of disease-causing lamin A mutants impairs the formation of DNA repair foci. Journal of Cell Science, 119 (13), 2704-2714.

34. Sekar, R. B., & Periasamy, A. (2003). Fluorescence resonance energy transfer (FRET) microscopy imaging of live cell protein localizations. Journal of Cell Biology, 160(5), 629-633. doi:10.1083/jcb.200210140

35. Miyawaki, A. (2003).Visualization of the Spatial and Temporal Dynamics of Intracellular Signaling. Developmental Cell 4, 295-305.

36. Aoki, K., Kiyokawa, E., Nakamura, T. & Matsuda, M. (2008). Visualization of growth signal transduction cascades in living cells with genetically encoded probes based on Forster resonance energy transfer. Philosophical Transactions of the Royal Society B: Biological Sciences 363, 2143-2151

37. Shcherbakova, D. M., Hink, M. A., Joosen, L., Gadella, T. W., & Verkhusha, V. V. (2012). An Orange Fluorescent Protein with a Large Stokes Shift for Single-Excitation Multicolor FCCS and FRET Imaging. Journal of the American Chemical Society, 134(18), 7913-7923. doi:10.1021/ja3018972

38. Tyas, L., Brophy, V. A., Pope, A., Rivett, A. J., & Tavaré, J. M. (2000). Rapid caspase-3 activation during apoptosis revealed using fluorescence-resonance energy transfer. EMBO Reports, 1(3), 266–270. doi: 10.1093/embo-reports/kvd050

39. Hyun, K., Jeon, J., Park, K., & Kim, J. (2017). Writing, erasing and reading histone lysine methylations. Experimental & Molecular Medicine, 49(4). doi:10.1038/emm.2017.11

40. He, C., Sun, J., Liu, C., Jiang, Y., & Hao, Y. (2019). Elevated H3K27me3 levels sensitize osteosarcoma to cisplatin. Clinical Epigenetics, 11(1). doi:10.1186/s13148-018-0605-x

41. Ishak, C. A., Marshall, A. E., Passos, D. T., White, C. R., Kim, S. J., Cecchini, M. J., Ferwati, S., Macdonald, W. A., Howlett, C. J., Welch, I. D., Rubin, S. M., & Mann, M. R., Dick, F. A. (2016). An RB-EZH2 Complex Mediates Silencing of Repetitive DNA Sequences. Molecular Cell, 64(6), 1074-1087. doi:10.1016/j.molcel.2016.10.021

42. Briand, N., & Collas, P. (2020). Lamina-associated domains: Peripheral matters and internal affairs. Genome Biology,21(1). doi:10.1186/s13059-020-02003-5

43. Guelen, L., Pagie, L., Brasset, E., Meuleman, W., Faza, M. B., Talhout, W., Meuleman, W., Eussen, B. H., Klein, A. D., Wessels, L., Laat, W. D.,Steensel, B. V. (2008). Domain organization of human

chromosomes revealed by mapping of nuclear lamina interactions. Nature, 453(7197), 948-951. doi:10.1038/nature06947

44. Gong, Y. (2018). Designing Principles for Epigenetic Fluorescent Resonance Energy Transfer Biosensors (Master's Thesis) . ProQuest Dissertations and Theses.